Sustainable synthesis of luminescent CdTe quantum dots coated with modified silica mesoporous nanoparticles: Towards new protein scavengers and smart drug delivery carriers

Elisabete Oliveira[†Ψ]*, Hugo M. Santos[†Ψ]*, Susana Jorge[†Ψ], Benito Rodríguez-González[§], Jessica Ariana-Machado, Fernando Novio[#], Julia Lorenzo[&], Daniel Ruiz-Molina[#], José L. Capelo[†Ψ] and Carlos Lodeiro[†Ψ]*.

[†] *Bioscope Group, UCIBIO-REQUIMTE, Chemistry Department, Faculty of Science and Technology, University Nova of Lisbon, Lisbon, Portugal*

[§] *Scientific and Technological Research Assistance Centre (CACTI), University of Vigo, Vigo, Spain*

[&]*Institut de Biotecnologia i Biomedicina, Departament de Bioquímica i de Biologia Molecular, Universitat Autònoma de Barcelona, Bellaterra, Barcelona, Spain*

[#]*Catalan Institute of Nanoscience and Nanotechnology (ICN2), CSIC and The Barcelona Institute of Science and Technology, Campus UAB, Bellaterra, 08193 Barcelona, Spain*

[Ψ]*Proteomass Scientific Society, Rua dos Inventores, Madan Park, 2829-516 Caparica, Portugal*

KEYWORDS. Luminescence, CdTe QDs, mesoporous silica nanoparticles, Doxorubicin, proteins, arthritis, prosthesis, nanoproteomics.

ABSTRACT

A novel family of luminescent nanoparticles, CdTeQDs@MNs, made of quantum dots coated by mesoporous silica is reported and fully characterized. While the presence of the luminescent QDs can allow for the imaging of the nanoparticles, as for instance to track their cell internalization, the mesoporous character of the silicon oxide coating simultaneously allows for the encapsulation and controlled release of different active principles such small molecules (rhodamine B), drugs such as doxorubicin and and isolated proteins (BSA, LYS, CA, OVA, LAC, Hb, Myb, CYT). Finally, and as a proof-of-concept to demonstrate the efficacy of these novel platforms, they have been used to extract and recognize proteins in raw serum of arthritis and prosthesis patients, without any previous protein depletion.

1. INTRODUCTION

Luminescent inorganic mesoporous silica nanoparticles (MNs) have emerged as a new generation of multifunctional systems with a broad range of applications in drug and gene delivery[1,2,3], biomedical imaging[1,4], photodynamic therapy[5,6], and photonic crystals (Insert reference). So, the design of multifunctional mesoporous silica nanoparticles for labeling, therapeutic use and for *in vivo* tumor imaging has become a hot topic of relevant scientific interest nowadays[1]. These nanoparticles can be easily tracked or monitored to evaluate their efficiency in drug delivery, as well as, in the encapsulation and adsorption of biomarkers, drugs and other important biomolecules[1,7,8].

The most common mesoporous silica nanoparticles used are based on MCM-41 or SBA-15, which are highly biocompatible, have low toxicity, high specific surface area, large pore volume, with hundred empty channels (mesopores) tunable pore structures, that can adsorb/encapsulate large amounts of bioactive molecules[9,10]. On the other side, among all fluorescent agents, inorganic quantum dots (QDs) are known to be 100 times more stable and up to 20 times brighter than traditional fluorescent dyes[11]. Due to their unique size-dependent optical and electronic properties, they are widely used for biological imaging and in electronic industries[12]. These materials are highly photostable, have size-tunable emissions, broad absorption and a narrow emission spectra, long fluorescence lifetime, high fluorescence quantum yield and high stability against photobleaching[13]. Usually the syntheses of QDs is done in organic solvents, using high temperatures (over 200ºC) and under a nitrogen atmosphere. Alternatively, aqueous synthesized QDs can be directly used for biological applications without any post-treatment, and the synthetic processes are cheaper, less toxic, simpler, more reproducible and environmentally friendly than the organometallic routes[14]. However, their bio-applications are sometimes limited

due to their oxidation with time, releasing heavy metal ions. Thus, coating QDs with silica shell also increases their biocompatibility.

QD-silica nanoparticles so far described involve the coating of quantum dots with solid silica,[15,16,17,18,19,20,21] while scarce examples of QDs covered with mesoporous silica nanoparticles (MNs) have been described[22]. In those cases, most often QDs are embedded into the mesoporous, bringing down any other possibility to further encapsulate active drugs or active components. So, these nanosystems are mostly modified at their surface with specific targets or linkers to be further applied in imaging or cell-specific targeting.[23,24] These limitations are even more relevant for their application with larger molecules, for instance, scavenging of proteins from complex biological samples (i.e., Serum) due to the size-exclusion effect of MNs pores. In such cases, the surface of these materials can be once more used to adsorb biomolecules through hydrophobic or electrostatic interactions,[16,25,26] while the encapsulation or extraction of proteins remains a challenge[27,28].

In this work, we have synthesized a green luminescent QD coated with a layer of surface unmodified mesoporous silica (CdTeQDs(**1**)@MNs) and explored it for the successful encapsulation and release of different active principles such small molecules (rhodamine B), drugs such as doxorubicin and and isolated proteins (BSA, LYS, CA, OVA, LAC, Hb, Myb, CYT). Moreover, and to demonstrate the viability of this synthesis for different QDs, an orange luminescent QD coated with a layer of surface unmodified mesoporous silica (CdTeQDs(**2**)@MNs) has also been obtained. Finally, and as a proof-of-concept to demonstrate the efficacy of these novel platforms for real situations, they have been used to extract and recognize proteins in raw serum of arthritis and prosthesis patients, without any protein depletion, a major challenge nowadays. Indeed, one of the main limitations of MNs to

encapsulate proteins is the pore size. Aware of this issue, Kros and co-workers[29] recently reported the design of mesoporous silica nanoparticles (MNs) with large pores based on Pluronic P123, which were able to encapsulate and release single proteins as α-lactalbumin, ovalbumin, bovine serum albumin, catalase, hemoglobin, lysozyme and cytochrome c. As a matter of fact, all MNs with large pore are SBA-15 (Pluronic P123)-based. Nonetheless, its nanosystem was only tested in seven isolated model proteins, and not in a complex biological sample. Some studies emphasize promising results in the use of MNs in the extraction and identification of endogenous peptides [30,31,32,33,34] , but due to the complexity of the samples, it always requires a pre-treatment, such as the removal of most abundant proteins from the serum.

2. MATERIALS AND METHODS

2.1. Materials.

Thioglycolic acid (TGA, ≥99%), $Cd(CH_3COO)_2.2H_2O$ (99.5%), Tetraethylorthosilicate (TEOS), Hexadecyltrimethylammonium bromide (CTAB, $C_{19}H_{42}BrN$, ≥98%), bovine serum albumin (BSA), lysozyme (LYS), bovine carbonic anhydrase (CA), ovalbumin (OVA), α-lactalbumin (LAC), human hemoglobin (Hb), Myoglobin from equine heart (Myb), cytochrome c from equine heart (CYT), doxorubicin (DOX) and Rhodamine (Rh) were purchased from Aldrich. Sodium borohydride ($NaBH_4$, 99%) and Ethylene glycol (≥99.5%) were from Fluka. Sodium tellurite (Na_2TeO_3, 99.5%) was from Alfa Aesar. Sodium hydroxide (NaOH) was from Panreac. Ammonium nitrate (NH_4NO_3) was acquired from Riedel Haën. Methanol (MeOH) was from Carlo Erba Reagents. All materials were used as received without further purification.

2.2.Preparation of cadmium telluride quantum dots (CdTeQDs)

Cadmium telluride quantum dots (CdTe QDs) were prepared by refluxing route accordingly with reference[37], but with some modifications. Briefly, to an aqueous solution containing 53 mg (0.2mmol) of $Cd(CH_3COO)_2$ was added 18µL of TGA and the pH adjusted to 10-11. After that, a solution of 8.86 mg (0.04 mmol) of Na_2TeO_3 was added to the previous mixture, followed by the addition of 80mg of $NaBH_4$. The final reactional mixture was refluxed at 100ºC under open-air conditions. Green (**1**) and Orange (**2**) CdTeQDs were obtained at different refluxing times.

2.3. Preparation of luminescent mesoporous silica nanoparticles (CdTeQDs@MNs).

Crude CdTe QDs (50mL), 100 mg cetylmethyl ammonium bromide (CTAB) (previously dissolved in 10mL of water) were heated at 50ºC for 30 minutes under stirring. After that, a mixture containing 30mL of water, 10 mL of ethylene glycol and 165 µL of NaOH was added and kept under stirring for another 30 minutes at 80ºC. Then, 0.75 µL of TEOS was added dropwise, and the final solution was stirred at 70ºC for 3 hours. The template was removed by the addition of ammonium nitrate in ethanol at 60ºC[38]. The final luminescent mesoporous nanoparticles were washed several times with water and ethanol. The same procedure was done with the amount of 50 mg of CTAB.

2.4. Nanoparticles Characterization

UV/Vis absorption spectra were recorded with a JASCO V-650 spectrophotometer and a NANODROP ND-1000. Fluorescence emission in a HORIBA Scientific FLUOROMAX-4 spectrofluorimeter and Infrared spectra in a FT-IR Spectrometer Spectrum two, UATR TWO PERKIN ELMER.

Fluorescence quantum yields[39] for green (**1**) and orange (**2**) CdTe QDs were measured using as standards fluorescein (ϕ=0.79)[40] and rhodamine (ϕ=0.70)[41] in ethanol. The values of fluorescence quantum yields were corrected accordingly with the different refraction indexes.

The nanoparticle size distributions and zeta potential were measured using a dynamic light scattering, a Malvern Nano ZS instrument with a 633 nm laser diode. Transmission electron microscopy (TEM) images were obtained in a JEOL JEM 2010F operating at 200 kV, TEM images were collected using a multiscan camera and Digital Micrograph software from Gatan. Energy-dispersive X-ray spectroscopy (EDS) data were obtained using an INCA 200 spectrometer from Oxford Instruments. Elemental maps were constructed combining the STEM unit with the EDS signal. Power X-ray diffraction (XRD) measurements were performed on a RIGAKU MiniFlex II using filtered CuKα radiation at 30 KV, 15 mA.

SEM images were obtained in a Quanta 650 FEG operating between 5-15 kV and 10^{-5} Pa of vacuum in the chamber. The samples were prepared by drop casting of the corresponding dispersion on aluminium tape followed by evaporation of the solvent at room temperature and pressure. Before analysis the samples were metalized with a thin layer of platinum, using a sputter coater (Leica Microsystems EM ACE600).

N_2 adsorption-desorption isotherms were recorded on a Micromeritics ASAP2010 automated sorption analyzer. The samples were degassed at 120^0C in vacuum overnight. The specific surface areas were calculated from the adsorption data in the low pressures range using the BET model. Pore size was determined following the BJH method.

2.5.Doxorubicin loading and released studies.

To solution of Doxorubicin (0.5 mg/mL) previously prepared in phosphate buffer (PBS) buffer pH 7.4, was collected 0.5 mL, which were mixed with 0.5 mL of green CdTeQDs@MNs and kept under stirring for 2 and 20 hours. The samples were centrifuged and the supernatant quantified by absorption in the NANODROP ND-1000. The encapsulation efficiency (EE%) and the loading capacity (mg/g) were determined by the same equations reported in **section 2.7.**

A similar procedure was also performed with rhodamine B.

The in vitro doxorubicin release of the encapsulated CdTeQDs(**1**)@MNs@DOX was performed by suspending the washed nanoparticles in a 2mL solution of PBS 7.4 and PBS 5.0 (final nanoparticles concentration= 0.5 mg/mL). All suspensions were stirred and kept at 37ºC. Aliquots at different times were collected and the free doxorubicin quantified by absorption in the NANODROP ND-1000.

2.6. In vitro studies in Hela cells

2.6.1. Cell culture: Human cervix adenocarcinoma HeLa cell line (ATC CCL-2) was maintained in a Minimum Essential Medium (MEM) alpha medium supplemented with 10% (v/v) heat inactivated fetal bovine serum (FBS) in a highly humidified atmosphere of 95% air with 5% C02 at 37◦C.

2.6.2. CLSM in vivo imaging of CdTeQDs(1)@MNs and CdTeQDs(1)@MNs@DOX in Hela cells: HeLa cells were trypsinized, counted, and adjusted to 1 × 105 cells mL−1 and 1 mL was added to each 35-mm2 Petri dish (MatTek, USA) for laser confocal microscopy. After 24 h, the dishes were incubated with medium alone as a negative control for fluorescence, and with 5 μg

of CdTeQDs@MNs or CdTeQDs(**1**)@MNs@DOX at 37 °C for 2 h. After being washed with fresh PBS (pH = 7.0) three times, 1mL of fresh medium was added and the cell nuclei and membrane were stained with Hoechst and

2.7. Protein encapsulation studies

Stock solutions (0.5 mg/mL) of Bovine Serum Albumin (BSA), Lysozyme (LYS), Carbonic Anhydrase (CA), Ovalbumin (OVA), α-lactalbumin (LAC), Hemoglobin (Hb), Myoglobin (Myb), Cytochrome c (CYT). A suspension of green (**1**) luminescent silica nanoparticles (CdTeQDs@MNs) (2mg/mL) in 1mL of PBS buffer was sonicated for 10 minutes. After that 0.5mL of proteins were mixed with 0.5 mL of green CdTeQDs@MNs. The final suspensions were stirred for 2 hours and 20 hours. The samples were centrifuged and the supernatant quantified by absorption in the NANODROP ND-1000. The encapsulation efficiency (EE%) and the loading capacity (mg/g) were determined by the following equations ($t_{protein}$: the total amount of protein/molecule; $f_{protein}$. Amount of free protein/molecule).

$$EE\% = \frac{t_{protein} - f_{protein}}{t_{protein}} \times 100 \qquad loading\ capacity\ \left(\frac{mg}{g}\right) = \frac{t_{protein\ (mg)} - f_{protein\ (mg)}}{amount\ of\ GCdTe@MNs}$$

2.8.Use of CdTeQDs@MNs for protein extraction

2.8.1. Serum samples

Human serum samples were obtained from arthritis patients, from patients with prosthesis and healthy controls. The individuals were of both genders and age ranged from 53 to 85 years. Prior to proteomic analysis, the serum samples were grouped into six pools of 25 samples each to reduce individual and biological variability. Table I summarizes the characteristics of each pool.

Condition	***Healthy controls***		***Arthritis***		***Prosthesis***	
Pool	**PC1**	**PC2**	**PA1**	**PA2**	**PP1**	**PP2**
No. of individuals	25	25	25	25	25	25
Female (%)	84	81	71	71	48	52
Age ± SD	67 ± 8	66 ± 8	70 ± 7	69 ± 7	66 ± 7	65 ± 6
Range of age	55 - 84	54 - 84	53 - 83	54 - 81	54 - 85	54 - 83

2.8.2. Protein Quantification

The total protein content was determined using a Bradford protein assay, using BSA as the standard protein.

2.8.3. CdTeQDs@ mesoporous silica protein fractionation

After protein quantification, 20 µL of each pool (1 mg of total protein) was mixed with 20 µL of green CdTeQDs@ mesoporous silica nanoparticles and incubated at room temperature in a shaker for 2 h. The pellet was then harvested by centrifugation at 17200 g during 5 minutes. Afterwards, the pellet was washed twice with 30 µL of milliQ water and harvested by centrifugation at 17200 g during 5 min.

2.8.4. Gel electrophoresis

Amounts of (i) 15 µg total protein for crude sample and for supernatant fraction and (ii) total pellet fraction were separately mixed with Laemmli Sample Buffer and loaded onto a 12.5%

SDS-PAGE, of 1 mm of thickness. After electrophoresis at 200 V during 50 min, gels were rinsed with milli-Q water and then stained overnight with colloidal Coomassie Blue G-250. Gels were rinsed with milli-Q water until a clear background was observed. Gel imaging was carried out with a ProPicII-robot (Digilab-Genomic Solutions, USA) using an exposure time of 16 ms and resolution of 70 µm.

2.8.5. In-gel protein digestion

Protein bands were excised manually and transferred to 0.5 mL low adhesion tubes, and then washed twice with water and then with 50% (v/v) acetonitrile/ 25 mM ammonium bicarbonate (ambic) until the blue colour disappeared. Gel bands were dehydrated with acetonitrile, then in-gel proteins were reduced with DTT (10 mM prepared in) at 37 ºC for 1 h and alkylated with IAA (55 mM) at room temperature for 45 min in the darkness. Subsequently, gel band were submitted to another washing steps and dehydration. Protein bands were incubated with trypsin (0.3 µg in 25 µL of 12.5 mM ambic/2% (v/v) acetonitrile) in an ice bath for 60 min in order to rehydrate the gel and to allow enzyme penetration into it. After this time, gel pieces were covered with 50 µL of 12.5 mM ambic and incubated for 12 h at 37 ºC. Finally, 25 µL of 5% (v/v) formic acid was added and the supernatants were transferred to new low adhesion tubes. Peptides were further extracted from the gel with 50% (v/v) acetonitrile/0.1% TFA. The samples were dried-down and stored at -60ºC until MALDI-TOF MS analysis.

2.8.6. In-gel protein digestion

Prior to analysis, sample were re-suspended in 10 µL of 0.3% (v/v) formic acid and 0.5 µL of sample was hand-spotted onto a MALDI target plate (384-spot ground steel plate) then 1 µL of a 7 mg/mL solution of α-cyano-4-hydroxycinnamic acid matrix in 0.1% (v/v) TFA and 50% (v/v)

ACN was added and allowed to air dry. Mass spectrometry data were acquired using an Ultraflex II matrix-assisted laser desorption/ionization tandem time-of-flight (MALDI-TOF/TOF) equipment (Bruker-Daltonics, Bremen, Germany) equipped with a LIFT cell and 50 Hz nitrogen laser. The mass spectrometer was operated in positive ion mode using a reflectron, and thus, spectra were acquired in the m/z range of 600-3500. A total of 500 spectra were acquired for each sample at a laser frequency of 50 Hz. External calibration was performed with the $[M + H]^+$ monoisotopic peaks of bradykinin 1-7 (m/z 757.3992), angiotensin II (m/z 1046.5418), angiotensin I (m/z 1296.6848) substance P (m/z 1758.9326), ACTH clip 1-17 (2093.0862), ACTH18-39 (m/z 2465.1983) and somatostatin 28 (m/z 3147.4710). Peptide mass fingerprints (PMF) were searched with the MASCOT search engine with the following parameters: (i) SwissProt Database2012_04 (535698 sequences; 190107059 residues); (ii) molecular weight of protein: all; (iii) one missed cleavage; (iv) fixed modifications: carbamidomethyl (C); (v) variable modification: oxidation of methionine and (vi) peptide tolerance up to 50 ppm after close-external calibration. The significance threshold was set to a minimum of 95% ($p \leq 0.05$). A match was considered successful when a protein identification score is located out of the random region, and the protein analysed scores first.

3. RESULTS AND DISCUSSION

3.1. Synthesis and characterization of green (1) and orange (2) CdTe-QDs and the derivatived CdTe-QDs@MNs hybrid nanoparticles

Green and orange luminescent CdTe QDs, samples **1** and **2** respectively, were obtained in aqueous solution in open air conditions at different refluxing times[37], using TGA as capping ligand and Na_2TeO_3 as tellurium source. This process avoided the synthesis of tellurium precursors from Te powder, which requires strict conditions, such as N_2 atmosphere, high temperatures, and organic solvents[42,43]. The absorption and emission maximum bands for the nanoparticles are centered at 510, 545 nm (green CdTe QDs) and 540, 585 nm (orange CdTe QDs), with very high fluorescent quantum yields of 80% and 25%, respectively (for more information see Supporting information, Table SN1). Absorption can be correlated with the size of the obtained quantum dots, based on the Yu and co-workers[43] equation:

$$D = (9.8127 \times 10^{-7})\lambda^3 - (1.7147 \times 10^{-3})\lambda^2 + (1.0064)\lambda - (194.84) \quad (1)$$

where λ is the absorption maximum. The estimated diameters obtained for green (**1**) and orange (**2**) quantum dots were of 2.6 and 3.2 nm, respectively. These estimated values are mostly in agreement with those obtained by dynamic light scattering (DLS) of 2.8±0.4 for (**1**) and, 7.5±1.2 (**2**), which as expected are slightly as long as they consider the hydrodynamic ratio. Regarding the zeta potential, the green QDs (-50±5 mV) are more stable than the orange QDs (-31±2 mV).

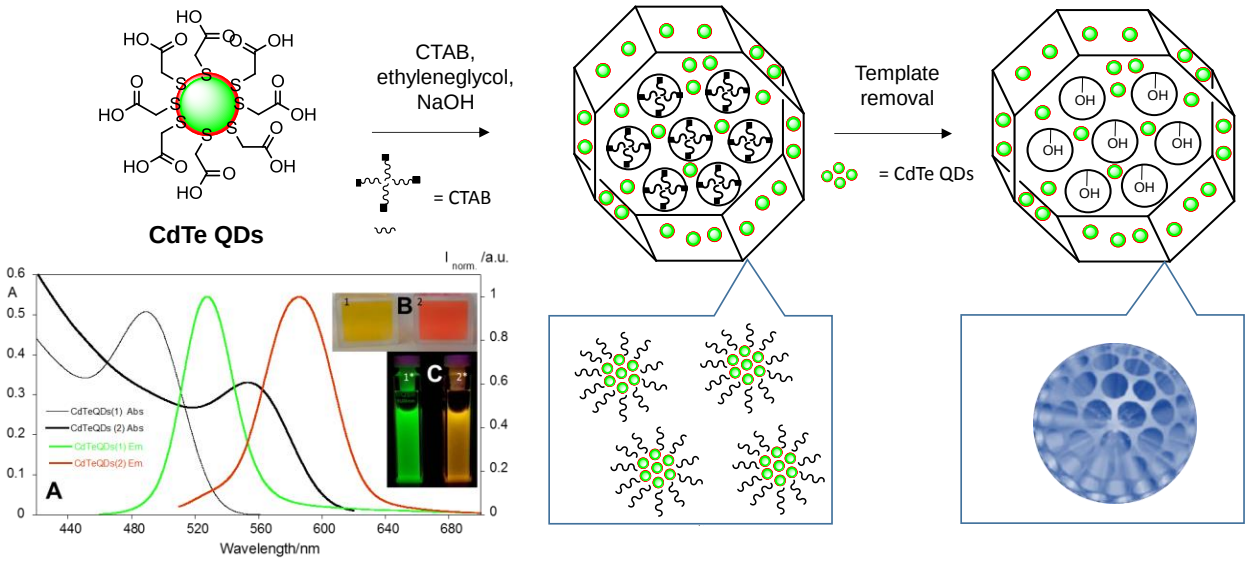

Figure 1. (Above) General synthetic pathway of CdTe Quantum Dots covered with mesoporous silica nanoparticles. (Bellow) **A.** Absorption and emission spectra of green (**1**) and orange (**2**) luminescent CdTe quantum dots in water (see characterization data in table SN1). **B** and **C**, naked-eye and under a UV lamp (λ_{exc}=365 nm) images of the CdTeQDs.

Luminescent mesoporous silica nanoparticles were obtained by encapsulation of CdTe QDs inside a silica matrix to generate mesoporous nanoparticles. Figure 1 illustrates the general synthetic process. In this synthesis, TEOS was used as a silica source, CTAB as cationic surfactant and template, ethylene glycol as a stabilizer and NaOH as a morphological catalyst. The MNs synthesis was based on the synthesis of MCM-41[44,45], but with the introduction of ethylene glycol. As expected the mesoporous nanoparticles obtained were of spherical shape (see figure 2) since the NaOH was used as the morphological agent. Moreover, the pore size of these hexagonal-symmetry nanoparticles showed to be higher than the common MCM-type materials, which have a pore size around 2-3 nm[1]. The effect of the CTAB concentration was also tested (see figures SN1-SN4) but the best results were achieved with the highest concentration. The final nanomaterials, the luminescent green (**1**) and orange (**2**) CdTeQDs covered with mesoporous nanoparticles were then obtained as a powder and were fully characterized by

fluorescence solid state, dynamic light scattering, FTIR, XRD, SEM, TEM (STEM) and EDS (see figure 2).

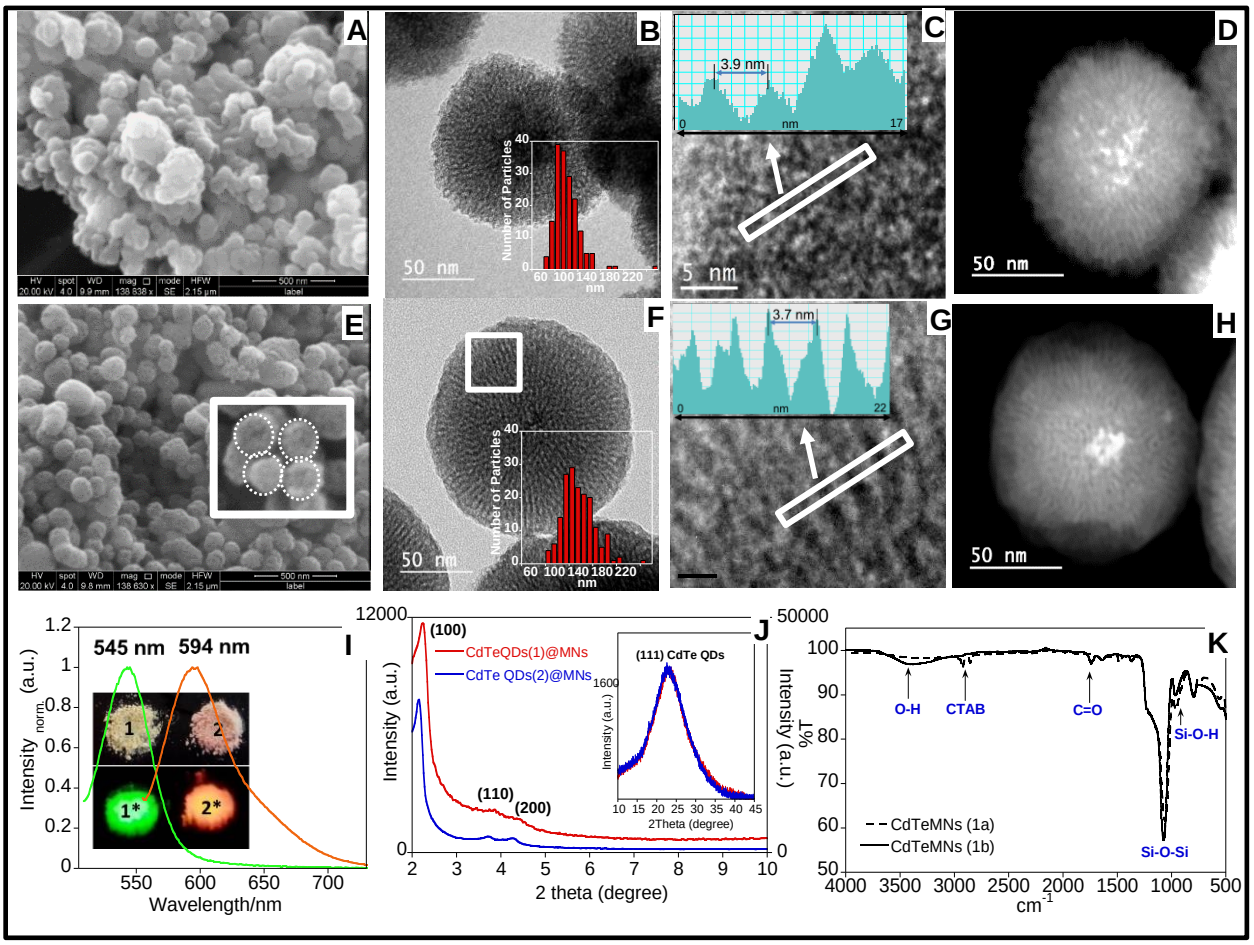

Figure 2. SEM images showing the quasi spherical shape of the green (**A**) and orange (**E**) CdTeQDs@MNs particles; (**B**) and (**F**) TEM images of two mesoporous nanoparticles (green MNs **B**, **C**; orange MNs **F**, **G**) showing the radial distribution of the pores, superimposed there is the corresponding size distribution of the particles; marked areas are enlarged in (**C**) and (**G**) together with the corresponding contrast profiles to aid in the measurement of pores size. (**D**) and (**H**) STEM images of two mesoporous nanoparticles (green MNs **D**; orangeMNs **H**) showing mass-thickness contrast, brighter areas in the core should correspond with areas containing higher z elements. (**I**) Fluorescence emission spectra in solid state, imagens under UV lamp and XRD spectra (**J**) of CdTeQDs(**1**)@MNs and CdTeQDs(**2**)@MNs. (**K**) FTIR spectra of CdTeQDs(**1**)@MNs with (**1a**) and without (**1b**) template.

SEM and TEM images clearly evidence the spherical shape of both nanosystems, as well as, the CdTe QDs covered by hexagonal-symmetry mesoporous silica nanoparticles. To accurately determine the size of the particles, TEM images were analyzed, and histogram for size and pore size were performed. The mesoporous nanoparticles present a diameter of ca. 105±8 nm (n=171) for CdTeQDs(**1**)@MNs and ca. 140±14 nm (n=173) for CdTeQDs(**2**)@MNs, with pore diameter values of *ca.* 3.9±0.3 nm and of *ca.* 3.7±0.2 nm for each nanosystem. In any case, the pore sizes obtained in these nanosystems are higher than the ones reported in the literature[1]. In figures 2 D and H we have included two HAADF-STEM images showing mass-thicknes contrast to demonstrate the core-shell nature of those mesoporous particles; in these images brighter areas should correspond with areas where higher z elements are present. Flyorescence characterization in solid state solid state revealed green and orange emissions (inset fig. 2I), with a maximum centered at 545 nm and 594 nm, and at the naked-eye color of white and lightly red, respectively.

The XRD analysis of CdTeQDs mesoporous silica nanoparticles shows the three typical low-angle reflections of a hexagonal array, which can be numbered as (100), (110) and (200) Bragg peaks[46]. These results suggest well-ordered mesoporous nanoparticles. The broad peak located in the range of 15-35º indicate the presence of amorphous silicon dioxide.[46] The maximum peak at 24.5º corresponds to the plane (111) of the cubic zinc blende structure of CdTe crystal[15]. The FTIR spectra (see figure 2K) of CdTe QDs@MNs shows the disappearance of the peaks centered at 2924 and 2852 cm^{-1} characteristics from CTAB, which confirms that the template was well removed. Moreover, characteristic peaks were identified at 3387 cm^{-1}, 1072 cm^{-1}, 965 cm^{-1} corresponded to the vibrations O-H, Si-O-Si, and Si-O-H, confirming the pure nature of mesoporous silica nanoparticles and the presence of silanol groups at its surface. The weak vibrational signal C=O also suggests that the CdTe QDs are totally embedded into the core of the

mesoporous silica nanoparticles. In order to obtain more precise information about the structure, surface and pore of the obtained luminescent silica mesoporous nanoparticles, nitrogen adsorption-desorption were carried out.

Figure 3 shows the nitrogen adsorption-desorption type IV isotherms of ordered mesoporous with an adsorption step behavior at P/P0 around 0.30-0.35. From these curves pore volumes of 0.29 cm^3/g and of 0.63 cm^3/g were calculated by the BJH model for green and orange MNs, on the adsorption branch of the isotherm. Through the application of the BET model, the average pore width and surface area were also estimated, where the pore width values of 35 Å and 33 Å, with surface areas of 438 m^2/g and 759 m^2/g were obtained for the systems CdTeQDs(**1**)@MNs and CdTeQDs(**2**)@MNs, respectively. Besides, the presence of mesoporosity in the synthetized systems, the BET surface areas and pore volumes are slightly lower than the traditional MCM-41 mesoporous nanoparticles, which is due to the presence of the luminescent quantum dots in the core these nanosystems. High-angle annular dark-field scanning TEM (HAADF-STEM) and STEM images confirm the presence and the localization of CdTe QDs in the center of the mesoporous silica nanoparticles, evidenced by the white contrast (see fig. 3A,C). In that images, the white points correspond to the elements of higher atomic number (CdTeQDs), whereas the majority are located in the center of the mesoporous silica nanoparticle. The composition of the nanosystem was further analyzed combining energy-dispersive X-ray spectroscopy with STEM unit (fig. 3 B, D). The obtained elemental maps clearly show the relative distribution of silica and cadmium, as can be seen by the green color (silica) and the oranges dots (cadmium) confirming once more the encapsulation of QDs in the center of the nanoparticle (fig. 3 B-D). The presence of the elements silica, cadmium and tellurium were also demonstrated in the EDS spectrum shown in fig. 3E,

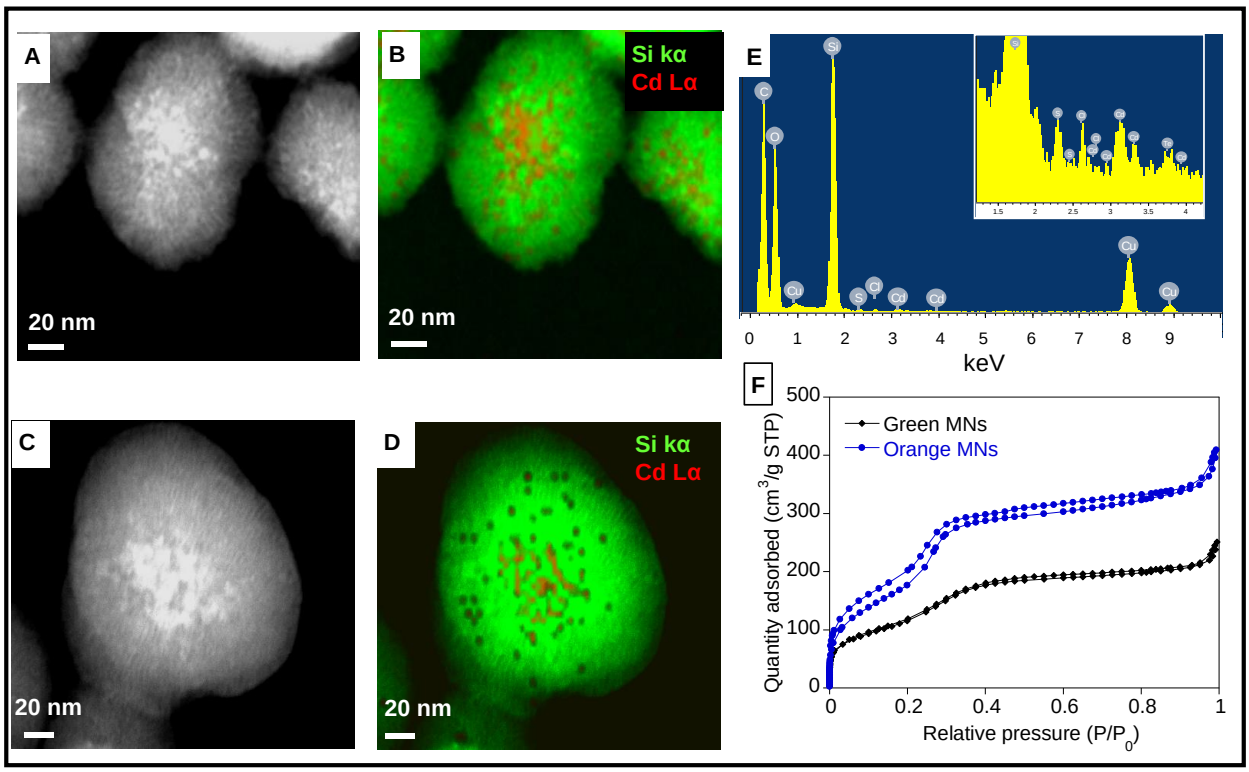

Figure 3. (A) and (C) STEM images of two mesoporous nanoparticles showing mass-thickness contrast together with the corresponding elemental mappings (B) and (C) demonstrating the core-shell geometry with the Si in green and Cd in red. (E) EDS spectrum obtained from an area comprising one entire particle, main elements are Si, O, S, Cl, Cd and Te; carbon are due to the contribution of the supporting film. (F) Nitrogen adsorption-desorption isotherms of green and orange CdTeQDs@MNs.

The dynamic light scattering results, revealed that both nanosystems are negatively charged, presenting zeta potential values of -6.5±0.8 mV CdTeQDs(**1**)@MSNs and -14±0.8 mV for CdTeQDs(**2**)@MSNs (see table SN2). The zeta-potential values are related to the presence of some colloidal instability since these nanossystems have a tendency to form aggregates with time. In order to improve their stability and at the same time evaluated their properties to extract and encapsulate proteins and their biological molecules selectively, CdTeQDs(**1**)@MNs

nanoparticles were incubated with isolated proteins, doxorubicin, rhodamine B and in serum/urine.

3.2.Doxorubicin loading/release and in vitro imaging studies in Hela cells.

As an exemplary study, the capability of the green luminescent mesoporous nanoparticles (CdTe(**1**) QDs@MNs) to load and release small molecules such as Rhodamine B (RhB) and Doxorubicin (DOX), an anticancer drug model, were first evaluated. The loading and release studies were initially performed in physiological pH (PBS, pH 7.4) media, wherein the molecules were incubated with the mesoporous nanoparticles (MNs) in weigth ratio of 1:4 (MNs:molecule) for incubation times of 2 and 20 hours. Encapsulation efficiency (EE%) and the amount adsorbed (mg/g) were determined accordingly with **section 2.5,** and the obtained results are gathered in figure 4A. The values obained for DOX were EE% (85%) and amount loaded (215 mg/g), which are much higher than those reported for others nanocarriers (for instance, EE% = 58.33%)[7]. Moreover, encapsulation turns out to be realtively fast as no significant differences were observed in the encapsulation and adsorption amounts taken at wo different incubation times of 2 and 20 hours. The corresponding drug release profile was performed in PBS pH 7.4 and 5.0 (fig.4B), where the drug release rate was favored at pH 5.0 against the pH 7.4 with percentages of 13% and 49%. It is worth to note that the release is fast, taking only 10 minutes. The procedure was followed during 72 hours, and no significant changes in the DOX amount released were verified.

As a proof-of-concept, the ability of this nanocarrier to enter in cells was evaluated in Hela cells and examined by confocal laser scanning microscopy (CLSM) at the excitation wavelength of

405 nm for the green mesoporous silica nanoparticles and 488 nm for DOX. For that purpose, Hela cells were incubated with the free nanocarrier CdTeQDs(**1**)@MNs and loaded with DOX in a concentration of 5 µg/mL for 24hours. The cytoplasmic membrane and the nucleus were stained with Cell Mask and DAPI, respectively. As can be seen in figure 4c, the free nanocarrier presents an intense green emission, confirming their stability inside cells, as well as the presence of DOX was confirmed by the red spots shown in figure SNX. Overall, this nanocarrier has the ability to penetrate in Hela cells, maintaining their fluorescence properties, with a consequent release of DOX.

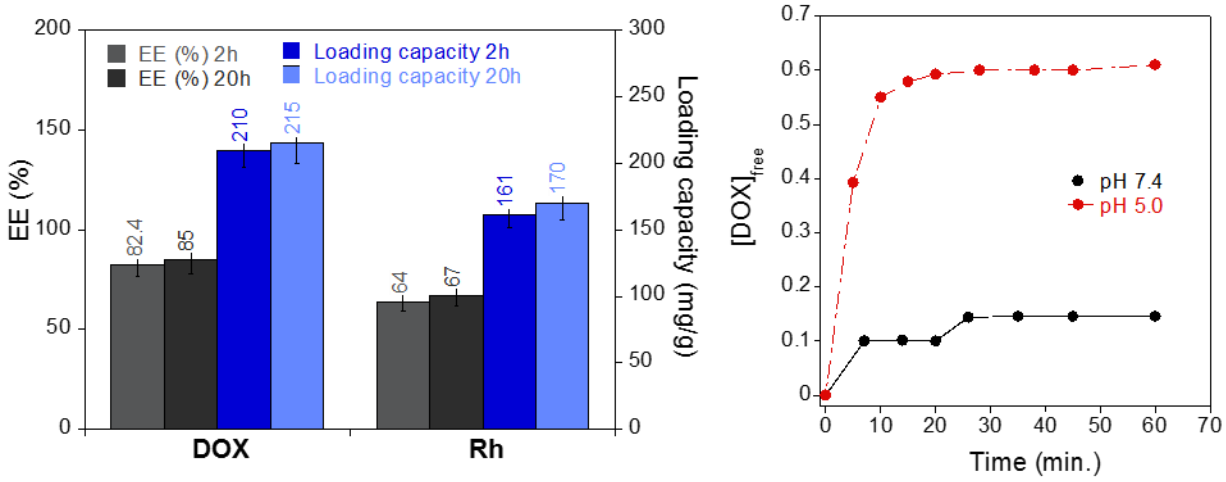

Figure 4. Cells images to complete this figure . Julia help in this part, I cannot open the imaris to perform this images. The samples correspond to S3 and S4, the S4 is loaded with DOX.

3.3.Protein encapsulation studies.

Encapsulation studies of the green mesoporous nanoparticles (CdTeQDs(**1**)@MNs) in physiological pH (PBS, pH 7.4) with single proteins exhibiting different sizes and pI, such as bovine serum albumin (BSA), lysozyme (LYS), carbonic Anhydrase (CA), ovalbumin (OVA),

α-lactalbumin (LAC), hemoglobin (Hb), myoglobin (Myb), cytochrome c (CYT) was accomplished. The proteins were incubated with the green mesoporous nanoparticles (MNs) in PBS, in a weight ratio of 1:4 (MNs:protein/molecule) for incubation times of 2 and 20 hours. Encapsulation efficiency (EE%) and the amount adsorbed (mg/g) were determined accordingly with **section 2.7,** and the obtained results are gathered in figure 5.

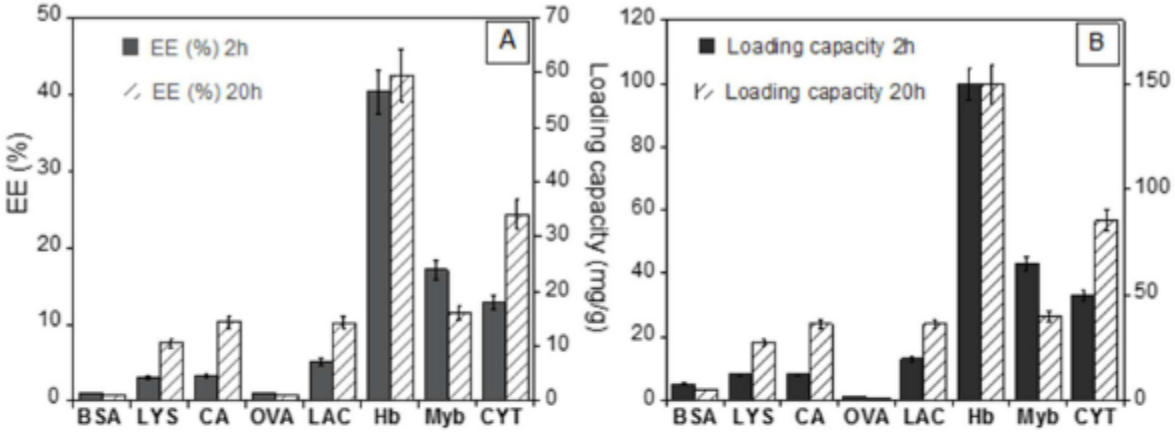

C

Proteins/ molecules	pI	Size (nm)	EE%		Amount adsorbed (mg/g)	
			2h	20h	2h	20h
BSA	4.9	7.3	0	0	0	0
LYS	10-10.5	2.9	3	11	8	27
CA	5.9	5.3	3	14	8	36
OVA	4.9	4.6	0	0	0	0
LAC	4.5	3.0	5	14	13	36
Hb	6.8	4.2	40	**60**	**100**	**150**
Myb	6.8	3.7	17	**30**	**43**	**40**
CYT	11.35	2.7	13	**34**	**33**	**85**

Figure 5. (A) Encapsulation efficiency (EE%) and corresponding loading capacity (mg/g) (B) of 8 model proteins in CdTeQDs(1)@MNs for a initial weigth ratio between protein and particles of 1:4 (250 mg of protein/1g particles). (C) Sctruture of heme groups in the metallo proteins Hb, Myb and CYT. (D) Data of encapsulation (EE%), loading capacity (mg/g), size and pI of the studied proteins.

As common tendency, an increase of the incubation time incubation contributes positively to the amount of protein adsorbed. Worth to mention also is the unrelevance of the carrier and protein charges on the encapsulation process. Indeed, Under the experiemental conditions used, CdTeQDs(**1**)@MNs nanoparticles present a negative charge with a zeta potential of ca. -14 mV. Accordingly with the isoelectric point, at pH 7.4 the proteins BSA, CA, OVA, LAC, Hb, Myb should be negatively charged wherea the CYT and LYS positively charged. Therefore, according with the charge balance, CYT and LYS should be preferably encapsulated (can this be due to the combiantion of other factors such as the size fo the proteins?). However, experimental results demonstrated that this is not the case; CdTeQDs(**1**)@MNs nanoparticles were able to encapsulate with the following protein yields: LYS(11%), CA (14%), LAC (14%), Hb (60%), Myb (30%) and CYT(34%). (see fig. 5 A, D). Surprisingly, these results indicate the tendency of these nanoparticles to encapsulate prefererably the metalloproteins Hb, Myb and CYT. The same behavoir was verified for the loading capacity, where a value around 150 mg/g was determined for Hb. These results may suggest the interaction (or afinnity) of the heme groups present in these proteins to the QDs nanoparticles core, being this interaction higher for Hb (Fig. 5).

3.4.Use of CdTeQDs@MNs for protein extraction

According to the excellent results previously described, the ability of CdTeQDs(**1**)@MNs nanoparticles for protein identification and extraction from complex biological samples, without previous protein depletion, was developed. As target samples, human serum samples from arthritis patients (PA), from patients with prosthesis (PP), and from healthy controls (PC) were used. The individuals were of both genders and ages ranged from 53 to 85 years. Before

proteomic analysis, the serum samples were grouped into six pools of 25 samples each to reduce individual and biological variability. Briefly, the CdTeQDs(**1**)@MNs nanoparticles were incubated in the target samples as reported previously in section 2.8.3. Afterwards, two fractions were obtained, such as the supernatant (SN) and the pellet (proteins attached to the nanoparticles, QD) (figure 6A). Both fractions were further submitted to a 1D-SDS-PAGE separation, where the resulted pool of peptides were analyzed by mass spectrometry. Figure 6B shows the 1D-SDS-PAGE of serum samples treated with and without the nanoparticles, and in a general way two different gel profiles are observed, one related to the supernatant and crude samples, which are quite similar between them, and another related to the pellet (the proteins attached to the nanoparticles). Moreover, visually there are no differences between healthy and unhealthy samples. However, after protein identification, 16 protein were found in the supernatant, and 13 in the pellet in the healthy control (PC). Regarding the PA and PP samples a total of 12, 17 proteins were identified in the supernatants, and 16, 13 proteins in the pellets (see figures 6D, SN5-SN7). In relation to the samples without fractionation with the nanoparticles and an average number of ca. 15-18 proteins were founded for PC, PA and PP; moreover the same behavior was detected of unique proteins with an average number of ca. 3 proteins (figures SN5, 6D). Remarkably, an increasing number of unique proteins was demonstrate with the use of the nanoparticles, where the unique proteins APOA4, SRPR in PC_QD, THRB, NCF1B, CFAH in PP_QD and CENPF, RN219, XIRP2, ANT3 in PA_QD were identified (see figure 6C). Interestingly, the proteins XIRP2 (Xin actin-binding repeat-containing protein2), the CENPF (centromere protein F), CO4B (complement C4-B) the RN219 (RING finger protein 219), HRG (Histidine-rich glycoprotein) and ANT3 (Antithrombin-III) were founded at the surface of the nanoparticles, but not in the supernatant or even the crude samples (without

CdTeQDs(1)@MNs). Thus, this fact reveals that the nanosystem CdTeQDs(**1**)@MNs works in the search and diagnosis of new biomarkers.

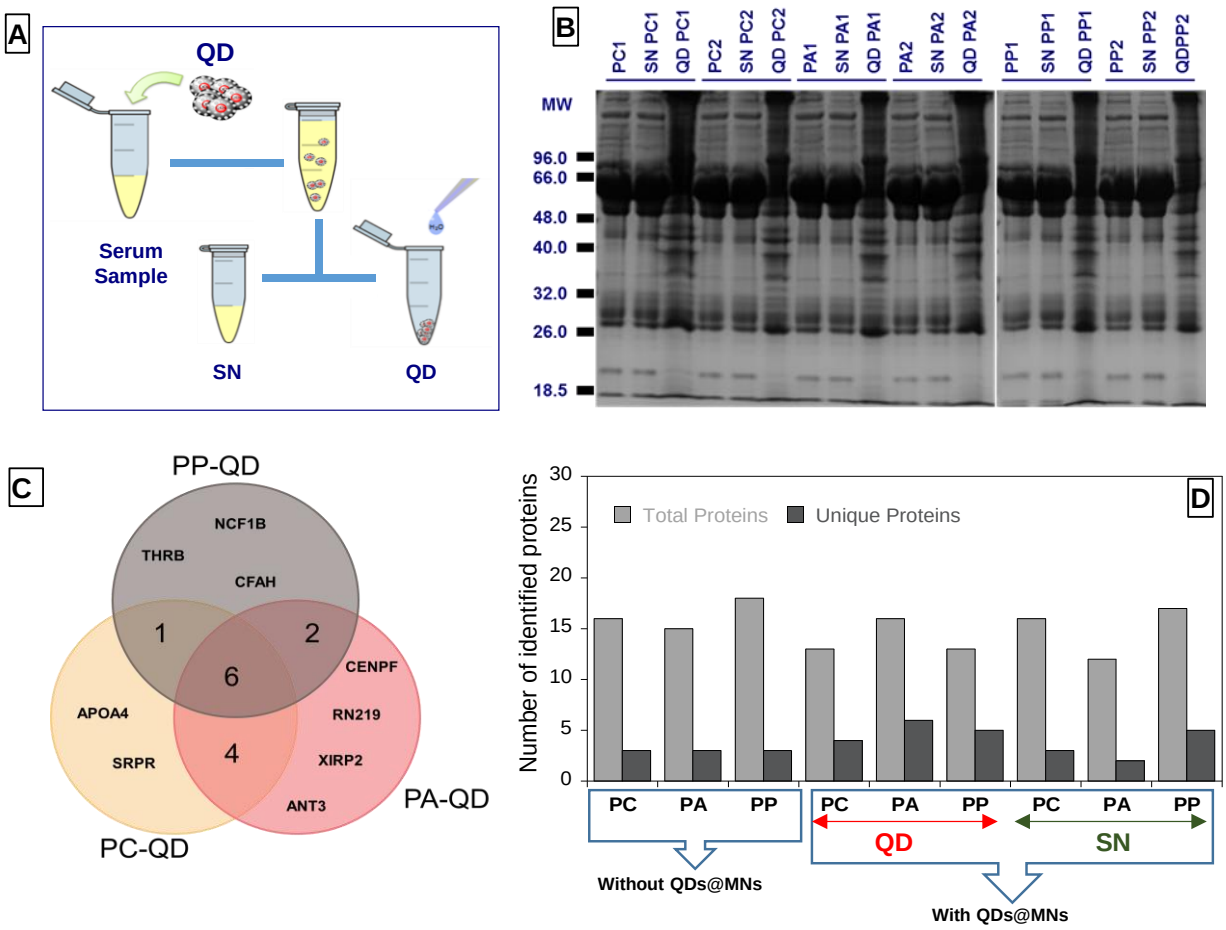

Figure 6. (A) General incubation procedure of CdTeQDs(**1**)@MNs **(QD)** with serum samples. **(B)** 1D-SDS-PAGE gel after CdTeQDs(1) @MNs (**QD**) fractionation for 3 different conditions, PC: Pool control; PA: pool of arthritis patients and PP: pool of patients with prosthesis. Pool 1 and 2 for each condition. QDs fractionation. Crude serum sample, SN: supernatant; and QD: quantum dots pellet. 15 µg of total protein in crude serum and SN fraction and pellet reconstituted in QD fraction. **(C)** Veen diagram showing the common and unique proteins founded in the surface of the nanoparticles for PC, PA and PP. **(D)** Number of total and unique identified proteins in PC, PA and PP with and without the use of nanoparticles CdTeQDs(**1**)@MNs **(QDs@MNs).**

4. CONCLUSION

A novel type of green and orange luminescent mesoporous nanoparticles, with sizes and pore sizes (ps.) of 105±8 nm (ps.3.9±0.3 nm) and 140±14 nm (ps.3.7±0.2 nm), respectively, were successfully synthetized and characterized. The green luminescent mesoporous nanoparticles (CdTeQDs(1)@MNs) reveled to be an excellent nanocarrier for drug delivery of doxorubicin in Hela cancer cells, whereas the release of doxorubicin is pH stimulated and this fact was evidenced inside the cells. This nanosystem (CdTeQDs(1)@MNs) showed to have a higher affinity for proteins with heme group (Hb) when it was tested with different isolated models of proteins. Overall, concerning complex samples, raw serum samples from osteoarthritis patients (PA), from patients with prosthesis (PP), and from healthy controls (PC), the nanosystem CdTeQDs(1)@MNs works as protein scavengers, identifying proteins that there were not founded in the supernatant or even in crude samples (without nanoparticles), facilitating then MALDI MS detection of CENPF, CO4B, RN219, HRG, ANT3 in human serum. These identified proteins are members of the pro-inflammatory complement cascade, including complement C3 and C4-B, which are extremely expressed and activated in human osteoarthritic joints, being then applied in the future as promising biomarkers.

ASSOCIATED CONTENT

(Word Style "TE_Supporting_Information"). **Supporting Information**. A listing of the contents of each file supplied as Supporting Information should be included. For instructions on what should be included in the Supporting Information as well as how to prepare this material for publications, refer to the journal's Instructions for Authors.

The following files are available free of charge.

brief description (file type, i.e., PDF)

brief description (file type, i.e., PDF)

AUTHOR INFORMATION

Corresponding Author

* E-mail: ej.oliveira@fct.unl.pt (Elisabete Oliveira), hmsantos@fct.unl.pt (Hugo M. Santos), cle@fct.unl.pt (Carlos Lodeiro)

Author Contributions

EO and HMS conceived and design the experiments; EO performed the synthesis, analysis and characterization of the nanomaterials. BR-G conducted the EDS, TEM, HAADF-STEM experiments. HMS and SJ applied the nanomaterials in proteomics. FN performed the XRD and SEM experiments. JAM and EO realized the encapsulation and release studies, and JL the imaging studies. JLC, CL, EO, DRM, JL contributed in the reagents, materials, analysis, and tools involved in this work. All authors discussed, analysed the data and contributed to the final version of the manuscript.

Notes

The authors declare no competing financial interest.

ACKNOWLEDGMENTS

This work was supported by the Unidade de Ciências Biomoleculares Aplicadas-UCIBIO which is financed by national funds from FCT/MEC (UID/Multi/04378/2013), Scientific PROTEOMASS Association (Portugal) and LAQV/REQUIMTE (UID/QUI/50006/2013). D.R-M and f.N. want to thanks project MAT2015-70615-R from the Spanish Government and by

FEDER funds. ICN2 acknowledges support from the Severo Ochoa Program (MINECO, Grant SEV-2013-0295). EO acknowledges the Post-Doctoral grant from Fundação para Ciência e Tecnologia (FCT-MEC) Portugal SFRH/BPD/108660/2015 and to Foundation L'Oreal (UNESCO and FCT) for the Prize For Women in Science 2015, "Medalhas de Honra L'Oréal Portugal para as Mulheres na Ciência".

REFERENCES

(1) Popat, A.; Hartono, S. B.; Stahr, F.; Liu, J.; Qiao, S. Z.; Qing (Max) Lu, G. Mesoporous Silica Nanoparticles for Bioadsorption, Enzyme Immobilisation, and Delivery Carriers. *Nanoscale* **2011**, *3* (7), 2801.

(2) Hartono, S. B.; Phuoc, N. T.; Yu, M.; Jia, Z.; Monteiro, M. J.; Qiao, S.; Yu, C. Functionalized Large Pore Mesoporous Silica Nanoparticles for Gene Delivery Featuring Controlled Release and Co-Delivery. *J. Mater. Chem. B* **2014**, *2* (6), 718–726.

(3) Kim, M.-H.; Na, H.-K.; Kim, Y.-K.; Ryoo, S.-R.; Cho, H. S.; Lee, K. E.; Jeon, H.; Ryoo, R.; Min, D.-H. Facile Synthesis of Monodispersed Mesoporous Silica Nanoparticles with Ultralarge Pores and Their Application in Gene Delivery. *ACS Nano* **2011**, *5* (5), 3568–3576.

(4) Wolfbeis, O. S. An Overview of Nanoparticles Commonly Used in Fluorescent Bioimaging. *Chem. Soc. Rev.* **2015**, *44* (14), 4743–4768.

(5) Shen, Y.; Shuhendler, A. J.; Ye, D.; Xu, J.-J.; Chen, H.-Y. Two-Photon Excitation Nanoparticles for Photodynamic Therapy. *Chem. Soc. Rev.* **2016**, *45* (24), 6725–6741.

(6) Wang, P.; Tang, H.; Zhang, P. Plasmonic Nanoparticle-Based Hybrid Photosensitizers with Broadened Excitation Profile for Photodynamic Therapy of Cancer Cells. *Sci. Rep.*

2016, *6*, 34981.

(7) Ge, K.; Zhang, C.; Jia, G.; Ren, H.; Wang, J.; Tan, A.; Liang, X.-J.; Zang, A.; Zhang, J. Defect-Related Luminescent Mesoporous Silica Nanoparticles Employed for Novel Detectable Nanocarrier. *ACS Appl. Mater. Interfaces* **2015**, *7* (20), 10905–10914.

(8) Chan, M.-H.; Lin, H.-M. Preparation and Identification of Multifunctional Mesoporous Silica Nanoparticles for in Vitro and in Vivo Dual-Mode Imaging, Theranostics, and Targeted Tracking. *Biomaterials* **2015**, *46*, 149–158.

(9) Tang, F.; Li, L.; Chen, D. Mesoporous Silica Nanoparticles: Synthesis, Biocompatibility and Drug Delivery. *Adv. Mater.* **2012**, *24* (12), 1504–1534.

(10) Shen, J.; Kim, H.-C.; Su, H.; Wang, F.; Wolfram, J.; Kirui, D.; Mai, J.; Mu, C.; Ji, L.-N.; Mao, Z.-W.; Shen, H. Cyclodextrin and Polyethylenimine Functionalized Mesoporous Silica Nanoparticles for Delivery of siRNA Cancer Therapeutics. *Theranostics* **2014**, *4* (5), 487–497.

(11) Chan, W. C.; Nie, S. Quantum Dot Bioconjugates for Ultrasensitive Nonisotopic Detection. *Science* **1998**, *281* (5385), 2016–2018.

(12) Medintz, I. L.; Uyeda, H. T.; Goldman, E. R.; Mattoussi, H. Quantum Dot Bioconjugates for Imaging, Labelling and Sensing. *Nat. Mater.* **2005**, *4* (6), 435–446.

(13) Resch-Genger, U.; Grabolle, M.; Cavaliere-Jaricot, S.; Nitschke, R.; Nann, T. Quantum Dots versus Organic Dyes as Fluorescent Labels. *Nat. Methods* **2008**, *5* (9), 763–775.

(14) Lu, Y.; Zhong, Y.; Wang, J.; Su, Y.; Peng, F.; Zhou, Y.; Jiang, X.; He, Y. Aqueous Synthesized near-Infrared-Emitting Quantum Dots for RGD-Based in Vivo Active Tumour Targeting. *Nanotechnology* **2013**, *24* (13), 135101.

(15) Dong, W.; Cheng, Y.; Luo, L.; Li, X.; Wang, L.; Li, C.; Wang, L. Synthesis and Self-

Assembly of Hierarchical SiO 2 –QDs@SiO 2 Nanostructures and Their Photoluminescence Applications for Fingerprint Detection and Cell Imaging. *RSC Adv.* **2014**, *4* (86), 45939–45945.

(16) Izak-Nau, E.; Voetz, M.; Eiden, S.; Duschl, A.; Puntes, V. F. Altered Characteristics of Silica Nanoparticles in Bovine and Human Serum: The Importance of Nanomaterial Characterization prior to Its Toxicological Evaluation. *Part. Fibre Toxicol.* **2013**, *10* (1), 56.

(17) Lu, M.; Zhang, W.; Gai, Y.; Yang, T.; Ye, P.; Yang, G.; Ma, X.; Xiang, G. Folate-PEG Functionalized Silica CdTe Quantum Dots as Fluorescent Probes for Cancer Cell Imaging. *New J. Chem.* **2014**, *38* (9), 4519–4526.

(18) Rampazzo, E.; Bonacchi, S.; Montalti, M.; Prodi, L.; Zaccheroni, N. Self-Organizing Core-Shell Nanostructures: Spontaneous Accumulation of Dye in the Core of Doped Silica Nanoparticles. *J. Am. Chem. Soc.* **2007**, *129* (46), 14251–14256.

(19) Wang, C.; Ma, Q.; Dou, W.; Kanwal, S.; Wang, G.; Yuan, P.; Su, X. Synthesis of Aqueous CdTe Quantum Dots Embedded Silica Nanoparticles and Their Applications as Fluorescence Probes. *Talanta* **2009**, *77* (4), 1358–1364.

(20) Wang, L.; Zhao, W.; Tan, W. Bioconjugated Silica Nanoparticles: Development and Applications. *Nano Res.* **2008**, *1* (2), 99–115.

(21) Wolcott, A.; Gerion, D.; Visconte, M.; Sun, J.; Schwartzberg, A.; Chen, S.; Zhang, J. Z. Silica-Coated CdTe Quantum Dots Functionalized with Thiols for Bioconjugation to IgG Proteins. *J. Phys. Chem. B* **2006**, *110* (11), 5779–5789.

(22) Gao, Y.; Dong, Q.; Lan, S.; Cai, Q.; Simalou, O.; Zhang, S.; Gao, G.; Chokto, H.; Dong, A. Decorating CdTe QD-Embedded Mesoporous Silica Nanospheres with Ag NPs to

Prevent Bacteria Invasion for Enhanced Anticounterfeit Applications. *ACS Appl. Mater. Interfaces* **2015**, *7* (18), 10022–10033.

(23) Chen, P.-J.; Hu, S.-H.; Hung, W.-T.; Chen, S.-Y.; Liu, D.-M. Geometrical Confinement of Quantum Dots in Porous Nanobeads with Ultraefficient Fluorescence for Cell-Specific Targeting and Bioimaging. *J. Mater. Chem.* **2012**, *22* (19), 9568.

(24) Zhang, S.; Wen, L.; Yang, J.; Zeng, J.; Sun, Q.; Li, Z.; Zhao, D.; Dou, S. Facile Fabrication of Dendritic Mesoporous SiO 2 @CdTe@SiO 2 Fluorescent Nanoparticles for Bioimaging. *Part. Part. Syst. Charact.* **2016**, *33* (5), 261–270.

(25) He, J.; Huang, M.; Wang, D.; Zhang, Z.; Li, G. Magnetic Separation Techniques in Sample Preparation for Biological Analysis: A Review. *J. Pharm. Biomed. Anal.* **2014**, *101*, 84–101.

(26) Katiyar, A.; Ji, L.; Smirniotis, P. G.; Pinto, N. G. Adsorption of Bovine Serum Albumin and Lysozyme on Siliceous MCM-41. *Microporous Mesoporous Mater.* **2005**, *80* (1–3), 311–320.

(27) Sun, J.; Zhang, H.; Tian, R.; Ma, D.; Bao, X.; Su, D. S.; Zou, H. Ultrafast Enzyme Immobilization over Large-Pore Nanoscale Mesoporous Silica Particles. *Chem. Commun.* **2006**, No. 12, 1322.

(28) Hartmann, M. Ordered Mesoporous Materials for Bioadsorption and Biocatalysis. *Chem. Mater.* **2005**, *17* (18), 4577–4593.

(29) Tu, J.; Boyle, A. L.; Friedrich, H.; Bomans, P. H. H.; Bussmann, J.; Sommerdijk, N. A. J. M.; Jiskoot, W.; Kros, A. Mesoporous Silica Nanoparticles with Large Pores for the Encapsulation and Release of Proteins. *ACS Appl. Mater. Interfaces* **2016**, *8* (47), 32211–32219.

(30) Tian, R.; Zhang, H.; Ye, M.; Jiang, X.; Hu, L.; Li, X.; Bao, X.; Zou, H. Selective Extraction of Peptides from Human Plasma by Highly Ordered Mesoporous Silica Particles for Peptidome Analysis. *Angew. Chemie* **2007**, *119* (6), 980–983.

(31) Tian, R.; Zhang, H.; Ye, M.; Jiang, X.; Hu, L.; Li, X.; Bao, X.; Zou, H. Selective Extraction of Peptides from Human Plasma by Highly Ordered Mesoporous Silica Particles for Peptidome Analysis. *Angew. Chemie Int. Ed.* **2007**, *46* (6), 962–965.

(32) Qin, H.; Gao, P.; Wang, F.; Zhao, L.; Zhu, J.; Wang, A.; Zhang, T.; Wu, R.; Zou, H. Highly Efficient Extraction of Serum Peptides by Ordered Mesoporous Carbon. *Angew. Chemie* **2011**, *123* (51), 12426–12429.

(33) Qin, H.; Gao, P.; Wang, F.; Zhao, L.; Zhu, J.; Wang, A.; Zhang, T.; Wu, R.; Zou, H. Highly Efficient Extraction of Serum Peptides by Ordered Mesoporous Carbon. *Angew. Chemie Int. Ed.* **2011**, *50* (51), 12218–12221.

(34) Qian, K.; Gu, W.; Yuan, P.; Liu, F.; Wang, Y.; Monteiro, M.; Yu, C. Enrichment and Detection of Peptides from Biological Systems Using Designed Periodic Mesoporous Organosilica Microspheres. *Small* **2012**, *8* (2), 231–236.

(35) López-Cortés, R.; Oliveira, E.; Núñez, C.; Lodeiro, C.; Páez De La Cadena, M.; Fdez-Riverola, F.; López-Fernández, H.; Reboiro-Jato, M.; Glez-Peña, D.; Luis Capelo, J.; Santos, H. M. Fast Human Serum Profiling through Chemical Depletion Coupled to Gold-Nanoparticle-Assisted Protein Separation. *Talanta* **2012**, *100*, 239–245.

(36) Araújo, J. E.; Lodeiro, C.; Capelo, J. L.; Rodríguez-González, B.; dos Santos, A. A.; Santos, H. M.; Fernández-Lodeiro, J. Novel Nanocomposites Based on a Strawberry-like Gold- Coated Magnetite (Fe@Au) for Protein Separation in Multiple Myeloma Serum Samples. *Nano Res.* **2015**, *8* (4), 1189–1198.

(37) Wu, S.; Dou, J.; Zhang, J.; Zhang, S. A Simple and Economical One-Pot Method to Synthesize High-Quality Water Soluble CdTe QDs. *J. Mater. Chem.* **2012**, *22* (29), 14573.

(38) Zhang, J.; Li, X.; Rosenholm, J. M.; Gu, H. Synthesis and Characterization of Pore Size-Tunable Magnetic Mesoporous Silica Nanoparticles. *J. Colloid Interface Sci.* **2011**, *361* (1), 16–24.

(39) Montalti M, Credi A, Prodi L, G. M. *Handbook of Photochemistry*; 3rd Ed. Taylor & Francis, B. R., Ed.; BOCA, 2006.

(40) Kellogg, R. E.; Bennett, R. G. Radiationless Intermolecular Energy Transfer. III. Determination of Phosphorescence Efficiencies. *J. Chem. Phys.* **1964**, *41* (10), 3042–3045.

(41) Arbeloa, F. L.; Ojeda, P. R.; Arbeloa, I. L. Flourescence Self-Quenching of the Molecular Forms of Rhodamine B in Aqueous and Ethanolic Solutions. *J. Lumin.* **1989**, *44* (1–2), 105–112.

(42) Dai, M.-Q.; Zheng, W.; Huang, Z.; Lanry Yung, L.-Y. Aqueous Phase Synthesis of Widely Tunable Photoluminescence Emission CdTe/CdS Core/shell Quantum Dots under a Totally Ambient Atmosphere. *J. Mater. Chem.* **2012**, *22* (32), 16336.

(43) Yu, W. W.; Qu, L.; Guo, W.; Peng, X. Experimental Determination of the Extinction Coefficient of CdTe, CdSe, and CdS Nanocrystals. *Chem. Mater.* **2003**, *15* (14), 2854–2860.

(44) Hom, C.; Lu, J.; Liong, M.; Luo, H.; Li, Z.; Zink, J. I.; Tamanoi, F. Mesoporous Silica Nanoparticles Facilitate Delivery of siRNA to Shutdown Signaling Pathways in Mammalian Cells. *Small* **2010**, *6* (11), 1185–1190.

(45) Cai, Q.; Luo, Z.-S.; Pang, W.-Q.; Fan, Y.-W.; Chen, X.-H.; Cui, F.-Z. Dilute Solution Routes to Various Controllable Morphologies of MCM-41 Silica with a Basic Medium †. *Chem. Mater.* **2001**, *13* (2), 258–263.

(46) Wu, C.; Chen, B.; Wang; Quan; Peng; Pan; Xu; Wu, C.; Wu. In Vitro and in Vivo Evaluation of Ordered Mesoporous Silica as a Novel Adsorbent in Liquisolid Formulation. *Int. J. Nanomedicine* **2012**, 199.